THE JOURNAL OF BIOLOGICAL CHEMISTRY
Vol. 275, No. 16, Issue of April 21, pp. 11964–11971, 2000

Printed in U.S.A.

X-ray Crystal Structure and Characterization of Halide-binding Sites of Human Myeloperoxidase at 1.8 Å Resolution*

(Received for publication, October 27, 1999, and in revised form, January 4, 2000)

Tristan J. Fiedler, Curt A. Davey‡, and Roger E. Fenna§

From the Department of Biochemistry and Molecular Biology, University of Miami Medical School, Miami, Florida 33136

The x-ray crystal structure of human myeloperoxidase has been extended to 1.8 Å resolution, using x-ray data recorded at −180 °C (r = 0.197, free r = 0.239). Results confirm that the heme is covalently attached to the protein via two ester linkages between the carboxyl groups of Glu^{242} and Asp^{94} and modified methyl groups on pyrrole rings A and C of the heme as well as a sulfonium ion linkage between the sulfur atom of Met^{243} and the β-carbon of the vinyl group on pyrrole ring A. In the native enzyme a bound chloride ion has been identified at the amino terminus of the helix containing the proximal His^{336}. Determination of the x-ray crystal structure of a myeloperoxidase-bromide complex (r = 0.243, free r = 0.296) has shown that this chloride ion can be replaced by bromide. Bromide is also seen to bind, at partial occupancy, in the distal heme cavity, in close proximity to the distal His^{95}, where it replaces the water molecule hydrogen bonded to Gln^{91}. The bromide-binding site in the distal cavity appears to be the halide-binding site responsible for shifts in the Soret band of the absorption spectrum of myeloperoxidase. It is proposed that halide binding to this site inhibits the enzyme by effectively competing with H_2O_2 for access to the distal histidine, whereas in compound I, the same site may be the halide substrate-binding site.

Myeloperoxidase (MPO, EC 1.11.1.7)[1] is a heme-containing enzyme found in mammalian neutrophils, where it catalyzes the hydrogen peroxide mediated peroxidation of halide ions (1, 2) and the pseudohalide thiocyanate (3, 4), according to the following reaction.

$$H_2O_2 + Cl^- + H_3O^+ = HOCl + 2H_2O$$

REACTION 1

Products of these reactions and their secondary metabolites are responsible for killing phagocytized bacteria and viruses (5, 6). MPO is one member of a gene family of mammalian peroxidases that also includes eosinophil peroxidase, lactoperoxidase (LPO), thyroid peroxidase, and prostaglandin H synthase (7–9).

The mature enzyme is a 140-kDa dimer of identical halves, each consisting of two polypeptide chains of 108 and 466 amino acids resulting from post-translational excision of 6 amino acids from a single polypeptide precursor (10, 11). Each half molecule contains a covalently bound heme that exhibits unusual spectral properties. The Soret band at 428 nm in the ferric enzyme is considerably red-shifted compared with other heme proteins, and relatively strong absorption bands in the visible region are responsible for the characteristic green color of the enzyme (12). Selective cleavage of a single disulfide bridge linking the two halves of MPO yields the hemi-enzyme that exhibits spectral and catalytic properties indistinguishable from those of the intact enzyme (13).

The overall protein fold of MPO was first revealed by a 3-Å resolution crystal structure of the canine enzyme (14). Apparently identical halves of the dimeric molecule are related by a noncrystallographic dyad axis and covalently linked by a single disulfide bridge at Cys^{153}. The secondary structure is largely α-helical, with very little β-sheet. Each half molecule consists of a central core of five helices and a covalently attached heme. Four of these helices derive from the large polypeptide and the fifth from the small. The remainder of the large polypeptide folds into four separate domains and a single open loop that surround the central core. The small polypeptide wraps around the surface of the molecule with only its carboxyl-terminal helix penetrating the interior to form part of the central core. A very similar protein fold has been found for the catalytic domain of the membrane-bound enzyme prostaglandin H synthase, which shares 22% sequence identity with MPO (15). Structure determination has confirmed the presence of a calcium-binding site and three sites of asparagine-linked glycosylation (Asn^{189}, Asn^{225}, and Asn^{317}) as well as the identities of the proximal His^{336} and distal His^{95}. However, the relatively low resolution (3 Å) did not allow full characterization of the covalent linkages between the heme and the protein. Details of these interactions and full characterization of the heme were later established by a 2.3-Å resolution crystal structure of the human enzyme (16). The heme was identified as a derivative of protoporphyrin IX in which the methyl groups on pyrrole rings A and C had been modified to allow formation of ester linkages with Glu^{242} and Asp^{94}, respectively. A third covalent link was identified as a sulfonium ion linkage between the sulfur atom of Met^{243} and the terminal β-carbon of the vinyl group on pyrrole ring A. Presence of the latter has been confirmed by mass spectrometric analysis of the heme released by autolytic cleavage and protease digestion (17).

The reaction between heme-peroxidases and hydrogen peroxide results in the formation of compound I, in which two oxidizing equivalents are stored as an oxyferryl Fe IV π-cation radical (18). In the case of MPO, this oxidized form of the enzyme is capable of either two-electron peroxidation of halide

* This work was supported by National Institutes of Health Grant GM 49149 (to R. E. F.). The costs of publication of this article were defrayed in part by the payment of page charges. This article must therefore be hereby marked "*advertisement*" in accordance with 18 U.S.C. Section 1734 solely to indicate this fact.

The atomic coordinates and structure factors (code 1cxp) have been deposited in the Protein Data Bank, Research Collaboratory for Structural Bioinformatics, Rutgers University, New Brunswick, NJ (http://www.rcsb.org/).

‡ Present address: Inst. fur Molekularbiologie and Biophysik, ETH-Honggerberg, HPM F4, CH-8093, Zurich, Switzerland.

§ To whom correspondence should be addressed: Dept. of Biochemistry and Molecular Biology, University of Miami Medical School, P.O. Box 016129, Miami, FL 33101. Tel.: 305-243-6564; Fax: 305-243-3065; E-mail: Rfenna@netscape.net.

[1] The abbreviations used are: MPO, myeloperoxidase; LPO, lactoperoxidase; PEG 8k, polyethylene glycol (average mass, 8 kDa).

TABLE I
Data collection and refinement statistics

	Native MPO		MPO-bromide	
	Total	Outer shell	Total	Outer shell
Resolution (Å)	50.0–1.75	1.81–1.75	50.0–1.75	1.81–1.75
No. of measurements	525,526		340,410	
Unique reflections	128,125		117,117	
I/σ	12.6	5.9	14.8	6.2
% completion	99.8	99.4	92.0	83.6
R-merge	0.053	0.220	0.060	0.194
Refinement res. (Å)	30.0–1.8	1.86–1.80	30.0–1.8	1.86–1.80
R-factor	0.197	0.266	0.239	0.293
R free	0.239	0.292	0.294	0.312

ions and thiocyanate or single-electron oxidation of a wide variety of aromatic alcohols and amines. The mechanism by which MPO catalyzes halide peroxidation is complex, because both H_2O_2 and halide are also inhibitors. Halide inhibition is competitive with respect to H_2O_2, and at any given pH there is an optimal ratio of the concentrations of halide: H_2O_2 consistent with maximal reaction velocity (19–22). The reaction of H_2O_2 with MPO to form compound I is pH-dependent. A group on the enzyme with a pK of 4.0 to 4.3, presumed to be the distal histidine, must be deprotonated for H_2O_2 binding to occur; whereas conversely, halide binding is favored at low pH when this group is protonated (23, 24). Spectral changes accompany the binding of halides to MPO. Fluoride, chloride, bromide, and iodide induce red-shifts of the Soret maximum from 428 nm to 435, 434, 432, and 423 nm, respectively, and measurements of these spectral changes have been used to determine the pH dependence of halide binding to the enzyme (19, 23). However, these studies have arrived at differing conclusions concerning the number of halide-binding sites on the enzyme and whether there are separate sites for halide binding as a substrate and as an inhibitor.

In this paper we present additional detailed information on the active site region of MPO as revealed by a structure determination of the human enzyme to 1.8 Å resolution, using x-ray diffraction data recorded at −180 °C. In addition, structure determination of an MPO-bromide complex has revealed a number of halide-binding sites, and their possible relevance to the catalytic mechanism of the enzyme is discussed.

EXPERIMENTAL PROCEDURES

Crystallization—Crystals of human MPO isoform C were grown by a method similar to those reported previously (25, 26). Hanging droplets containing 20 mg/ml MPO, 50 mM sodium acetate (pH 5.5), 50 mM ammonium sulfate, 2 mM calcium chloride, and 6% (w/v) PEG 8k were equilibrated with reservoirs containing the same concentrations of the above salts but with 22 to 25% w/v PEG 8k at 65 °F. Crystals were transferred to protein-free substitute mother liquor containing the above salts and 16% w/v PEG 8k for crystallographic experiments. For low temperature data collection, 20% (w/v) 2-methyl 2,4-pentanediol was included as cryoprotectant.

Data Collection and Processing—X-ray diffraction data were recorded using a 30-cm MAR image plate detector (MAR Research, Hamburg, Germany) mounted on a Rigaku RU300 x-ray generator equipped with long focusing mirrors (Area Detector Systems Corp., Poway, CA). A native low temperature (−180 °C) diffraction data set to 1.8 Å resolution was recorded from a single crystal, flash-frozen in a stream of cold nitrogen from a crystal cooling device (Area Detector Systems Corp.). The crystal to detector distance was set at 115 mm, and 231 frames of data were recorded at 1° rotation intervals. Image processing and data scaling were performed with DENZO and SCALEPACK (27). The crystals belong to space group $P2_1$ with a single dimeric molecule of MPO as the asymmetric unit. Unit cell parameters from the frozen crystal were: a = 110.0 Å, b = 63.4 Å, c = 92.2 Å, β = 97.4°, compared with values of a = 111.7 Å, b = 64.6 Å, c = 94.2 Å, β = 97.9° at room temperature (16), indicating significant shrinkage of the unit cell at cryogenic temperature. Data collection and scaling statistics are given in Table I.

Structure Determination and Refinement—The starting model for refinement was the 2.3 Å resolution structure of human MPO represented in the Rutgers University Protein Data Bank under access code 1MHL (16). This model consists of 9424 nonhydrogen protein atoms and 423 water molecules. The crystallographic *R*-factor was 15.0% for 55,500 reflections (93% completion) in the resolution range 6.0 to 2.28 Å, with root mean square deviations from ideality for bond lengths and angles of 0.013 Å and 3.01°. Refinement using the 1.8 Å resolution low temperature data set was carried out using X-PLOR version 3.8 (28) and stereochemical parameters derived from Engh and Huber (29). Cycles of simulated annealing, conjugate-gradient energy minimization, and isotropic temperature factor refinement were performed between stages of model rebuilding using $2F_o - F_c$ and $F_o - F_c$ maps in conjunction with the molecular modeling program TURBO (Bio-Graphics Inc., Marseille, France). The highest resolution of x-ray data included in the refinement was increased stepwise from 2.25 Å to 2.0, 1.85, and 1.8 Å. A subset comprising 5% of the reflections was not used in refinement to allow for calculation of a free *R*-factor (30). Additional water molecules were included in the model when observed as spherical peaks at a level of at least 4 σ in Fo-Fc difference maps, provided that suitable hydrogen bonding partners were already present in the model. Water molecules that failed to reappear at 2 σ in $2F_o - F_c$ maps following a round of refinement were removed from the model. Because of an ambiguity in the hydrogen bonding pattern for water molecules in the distal heme cavity in the 2.3 Å resolution structure of human MPO, all water molecules in the distal cavity were specifically excluded from the model until the late stages of refinement when their positions could be clearly determined from $F_o - F_c$ difference maps. Also, toward the end of refinement, solute ions, including acetate and sulfate were added to the model where indicated by additional difference map density and the presence of suitable protein ligands. Noncrystallographic symmetry restraints were not used during refinement, but a bulk solvent model was included in the final stages and resulted in considerable improvement in the *R*-factor for data in the lowest resolution shell. The quality of the model was assessed using the program PROCHECK (31). Coordinates for the final model have been deposited with the Rutgers University Protein Data Bank, access code 1CXP.

Bromide-substituted Crystals—A crystal of human MPO was transferred to substitute mother liquor consisting of 16% PEG 8k, 50 mM sodium acetate (pH 5.5), 50 mM ammonium sulfate, 2 mM calcium acetate, and 20 mM sodium bromide. Following equilibration for 48 h. the crystal was washed briefly in the same mother liquor with 20% (v/v) 2-methyl 2,4-pentanediol added as cryoprotectant before flash freezing in a stream of nitrogen at −180 °C. X-ray diffraction data were recorded as described for the native enzyme and scaling statistics are given in Table I. The positions of bound bromide ions were determined from a difference Fourier map using $F_{o\,(MPO\text{-}bromide)} - F_{c\,(MPO)}$ as coefficients. Subsequently, bromide ions were included in the model, and refinement of the structure was carried out using X-PLOR version 3.8 as described above. Coordinates for the refined model of the MPO-bromide complex have been deposited with the Rutgers University Protein Data Bank under access code 1D2V.

RESULTS

Quality of the Refined Native MPO Model—The final model consists of 10,307 nonhydrogen atoms, including 1140 amino acids, 2 hemes, 16 sugars, 2 calcium ions, 2 chloride ions, 4 sulfates, 6 acetates, and 838 water molecules. The crystallographic *R*-factor for reflections in the 30 to 1.8 Å range is 19.7%, and the corresponding free *R*-factor is 23.9%. The root mean square deviations from ideality for bond lengths and angles are 0.013 Å and 1.23°. A Ramachandran plot for the

whole molecule shows 88.8% of residues in the most favored regions and 11% in additionally allowed regions. Ser^{42} in both halves of the molecule has φ,ψ angles in the generously allowed region, and no residues fall in disallowed regions. Although the φ,ψ angles for Ser^{42} lie outside of the additionally allowed region, the orientation of this residue appears to be influenced by hydrogen bonding between the NH and CO groups of both of its adjacent peptide bonds with amino acid side chains. There are three *cis*-prolines at positions 124, 355, and 558 and a *cis*-peptide bond between Asn^{549} and Asn^{550} in each half of the molecule. Stereochemical parameters for both the main chain and side chains were determined to be within, or better than, the ranges given for other protein structures determined at comparable resolution according to the program PROCHECK (31).

Because the two halves of the MPO molecule (designated A and B) have different environments in the crystal, there are some differences in the conformations of equivalent side chains on the surface of the molecule. In general, the A half of the molecule is involved in more extensive intermolecular contacts in the crystal, and for this reason is a little better ordered than the B half. This is reflected in the lower average B-factor for protein atoms in the A half (11.1 $Å^3$) compared with the B half (13.1 $Å^3$). The amino acid numbering system used here is based on designating the first Cys in the small polypeptide as residue 1 (14). In the sequence of human MPO, deduced from the cDNA, there are 2 residues (Val and Thr) prior to Cys^1 (32, 33), but these are not evident in the electron density map.

The backbone density is very well defined for all four polypeptide chains, except for two surface loops involving residues 217–218 and 354–356 in both halves of the molecule. The amino terminus of the small polypeptide (residues 2–6) is poorly ordered in the A half but well ordered in the B half where the side chains of Glu^3 and Gln^4 are involved in hydrogen bonding with residues in a symmetry-related molecule. Conversely, the carboxyl terminus of the large polypeptide (residues 576–578) is poorly ordered in the B half but well defined in the A half where the terminal carboxyl group is hydrogen bonded to the amide nitrogen of Gln^{75} in a neighboring molecule. A number of side chains on the surface of the molecule (15 in the A half and 23 in the B) exhibit some degree of disorder, although in many cases this is limited to truncated density for the termini of the longer side chains of arginine and lysine.

Structural Features of MPO—The overall polypeptide fold for human MPO (Fig. 1) is the same as reported previously for the dog enzyme (14) and described briefly in the introduction. However, the higher resolution of the current electron density map has allowed more detailed characterization of a number of structural features. The calcium-binding site has typical pentagonal bipyramidal coordination. The Oγ of Ser^{174} and the peptide carbonyl oxygen of Phe^{170} provide the axial ligands, whereas the other five ligands (Asp^{96} carboxyl oxygen and peptide carbonyl oxygen, Thr^{168} hydroxyl and peptide carbonyl oxygens, and Asp^{172} carboxyl oxygen) are arranged approximately co-planar. Five of these ligands arise from residues within the 168–174 loop of the large polypeptide, whereas the other two involve Asp^{96}, which is adjacent to the distal His^{95} in the small polypeptide. The orientations of all of the sugars comprising the Asn^{317} glycosylation site have been determined. The carbohydrate chain consists of the standard $(GlcNac)_2$-$(Man)_3$ structure with a fucose 1–6 linked to the first GlcNac. Interactions between these sugar chains in the two halves of the molecule make up much of the dimer interface in MPO. Details of the carbohydrate conformation and its interactions with the protein will be presented elsewhere.

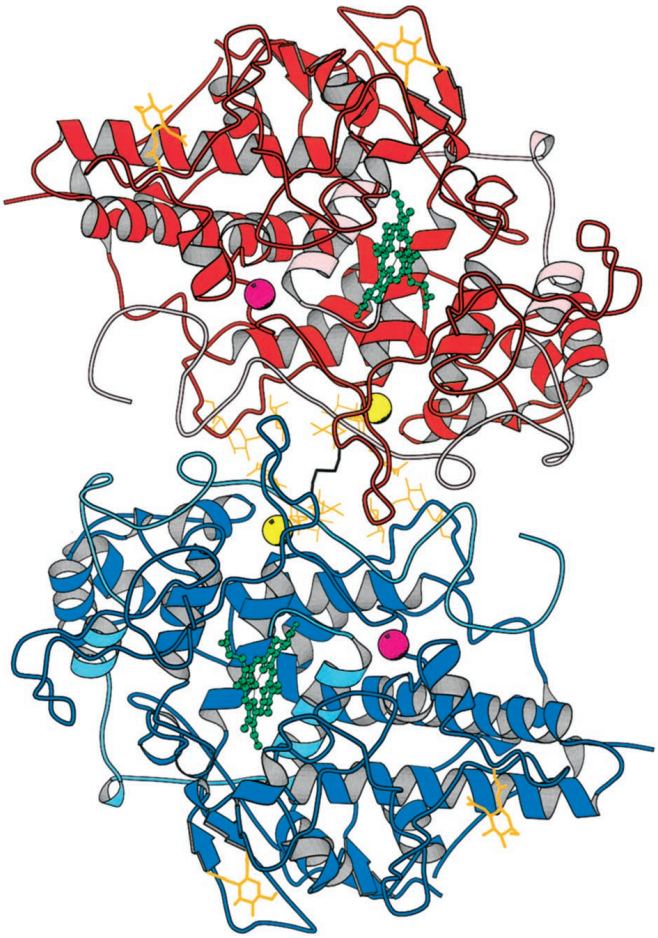

FIG. 1. **Entire MPO dimer, viewed along the molecular dyad axis.** The large polypeptides of the two halves are colored *red* and *blue*, whereas the small polypeptides are in *lighter shades* of the same colors. Other color coded features include: hemes (*green*), carbohydrate (*orange*), calcium (*purple*), and chloride (*yellow*). At the center of the molecule the disulfide linking the two halves is shown in *black*.

Heme Structure and Interactions with the Protein—The heme group is a derivative of protoporphyrin IX in which the methyl groups on pyrrole rings A and C have been modified to allow formation of ester linkages with the carboxyl groups of Glu^{242} and Asp^{94}, respectively. In addition the β-carbon of the vinyl group on pyrrole ring A forms a covalent bond with the sulfur atom of Met^{243}, giving rise to a sulfonium ion linkage (Fig. 2). The resulting positive charge on the sulfur atom does not appear to be involved in any additional electrostatic interactions with the protein. The heme porphyrin ring is considerably distorted from planarity. Although pyrrole rings B and D are nearly co-planar, ring A and, to a lesser degree, ring C are tilted toward the distal side, resulting in a bow-shaped structure for the heme. Because of these distortions to the porphyrin ring, it is impractical to define the position of the central iron atom with respect to a "heme plane" as is commonly reported for heme-containing proteins. However, the iron is positioned slightly to the proximal side, 0.2 Å below a line connecting the nitrogen atoms of pyrrole rings B and D. The N_ϵ of His^{336} provides the proximal ligand to the iron, with an iron to nitrogen distance of 2.19 Å, whereas the N_δ of this residue is hydrogen bonded to the amide carbonyl oxygen of Asn^{421}.

The carboxyl groups of both of the heme propionates also make electrostatic interactions with the protein. The ring D propionate interacts with the guanidinium groups of both Arg^{333} and Arg^{424}, and also forms a hydrogen bond with a water molecule. The ring C propionate interacts with both

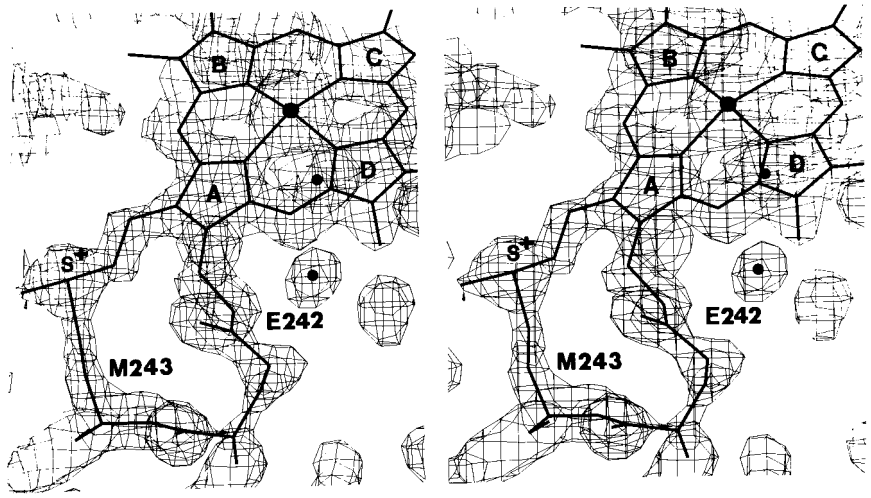

FIG. 2. **Stereo view of a $2F_o - F_c$ omit map calculated using phases from a model from which the side chains of Glu^{242} and Met^{243}, as well as the pyrrole ring A methyl carbon and both of the vinyl carbons were removed from the model prior to a cycle of simulated annealing refinement.** The map, contoured at 1.4 σ, shows electron density for the sulfonium ion linkage between the sulfur atom of Met^{243} and the β carbon of the pyrrole ring A vinyl group as well as the ester linkage between Glu^{242} and the methyl carbon.

TABLE II
Heme-protein interactions

Heme group	Residue	Bond type	Distance	
			A	B
			Å	
A methyl C	Glu^{242} O_ε	covalent	1.55	1.55
A vinyl Cβ	Met^{243} S	covalent	1.63	1.62
C methyl C	Asp^{94} O_δ	covalent	1.54	1.55
C propionate O1	Thr^{100} O_γ	H-bond	2.91	2.92
C propionate O1	Asp^{98} O_δ	H-bond	2.68	2.67
C propionate O2	Thr^{100} NH	H-bond	2.81	2.76
C propionate O2	Wat^{846} OH	H-bond	2.58	2.81
D propionate O1	Arg^{424} NH_2	H-bond	2.94	2.94
D propionate O1	Wat^{798} OH	H-bond	2.63	2.70
D propionate O2	Arg^{333} NH_1	H-bond	2.84	2.73
D propionate O2	Arg^{424} N_ε	H-bond	2.86	2.85
Fe^{3+}	His^{336} N_ε	ligand	2.19	2.19
Fe^{3+}	Wat^{1} OH	ligand	2.90	3.00

Asp^{98} and Thr^{100}. One of the propionate oxygens forms hydrogen bonds with the Thr^{100} peptide NH and additionally with a water molecule, whereas the other hydrogen bonds with the carboxyl group of Asp^{98}. Distances for these interactions and the heme-protein covalent bonds are given in Table II.

Distal Heme Cavity—Access to the distal cavity occurs via a narrow oval-shaped opening with a predominantly hydrophobic surface above pyrrole ring D. The pyrrole ring forms the base of the opening, whereas the upper surface consists of the β, γ, and δ carbons of Arg^{239} and phenylalanines 99, 366, and 407 make contributions to the lateral surfaces of the opening. A funnel-shaped channel filled with water molecules leads from this narrow opening to the surface of the protein. The distal heme cavity is occupied by the side chains of Gln^{91}, His^{95}, and Arg^{239}, together with five water molecules (W1–W5). Each of these three side chains is hydrogen bonded to a different water molecule, whereas a fourth water molecule is hydrogen bonded to the heme pyrrole ring C propionate. Additional hydrogen bonding occurs between these water molecules as indicated in Fig. 3. A fifth water molecule (W5) is hydrogen bonded to W2 and possibly also weakly to W3. The distal His^{95} is hydrogen bonded to W1, which is positioned approximately mid-way between its N_ϵ and the heme iron. Its distance from both the histidine nitrogen and the iron (2.9 Å) suggests that it is hydrogen bonded to the histidine and is not strongly coordinated to the heme iron. The amide nitrogen of Gln^{91}, at the back of the distal cavity, is hydrogen bonded to W2 as well as to the carbonyl oxygen of the ester bond between Glu^{242} and the heme pyrrole ring A methyl carbon. The amide oxygen of Gln^{91} is in turn hydrogen bonded to the amide nitrogen of Gln^{88}. The guanidinium group of Arg^{239} is hydrogen bonded to W3 but additionally forms a salt bridge with the carboxyl group of Asp^{237} as well as a hydrogen bond with the peptide carbonyl oxygen of Asp^{98}.

As shown in Fig. 4, a chain of hydrogen bonds involving 5 buried water molecules and the side chain of His^{250} extends from the distal histidine to the surface of the molecule, at a point remote from the solvent channel leading to the distal cavity. The N_δ of the distal His^{95} is hydrogen bonded to a buried water molecule, which is separated from the distal cavity water molecules by the imidazole ring. This water is also hydrogen bonded to N_ϵ of His^{250}, thereby forming a bridge between the two histidines. The N_δ of His^{250} is hydrogen bonded to a second water molecule, which is the first in a chain of four buried water molecules, linked by hydrogen bonds, and leading to the surface of the protein. Each of the five buried water molecules is additionally hydrogen bonded to an oxygen acceptor. The first is a carboxyl oxygen of Asp^{237}, whereas the other four are all peptide carbonyl oxygens.

Characterization of a Halide-binding Site—Toward the end of refinement, the most significant feature seen in $F_o - F_c$ residual maps was additional positive density (11 σ) at a modeled water molecule hydrogen bonded to the peptide NH groups of Trp^{32} and Val^{237} in both halves of the molecule. Because Val^{237} is close to the amino terminus of an α-helix (residues 326–338), a bound anion in this location could interact with the partial positive charge associated with the helix dipole. Of the anions present in the mother liquor of crystallization (50 mM acetate, 50 mM sulfate, 2 mM chloride) chloride best modeled the observed compact spherical density. When chloride was

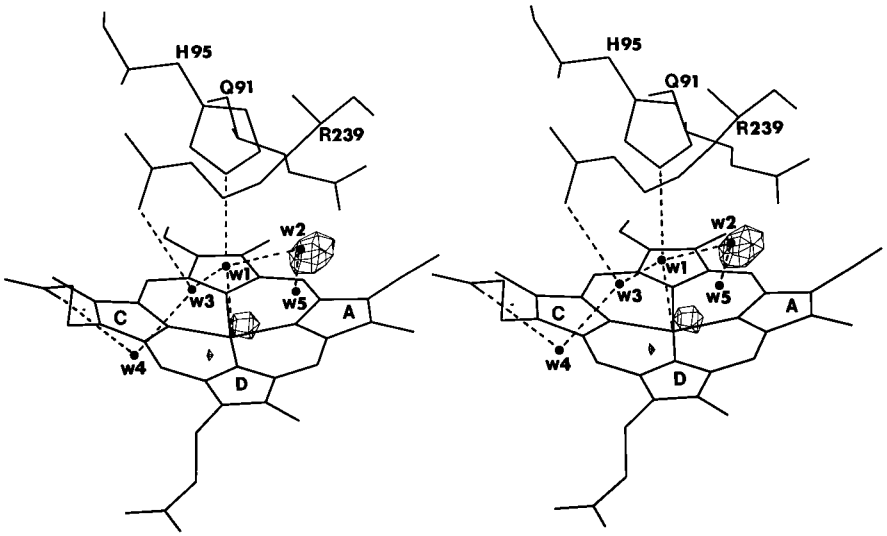

FIG. 3. **Stereo view of the hydrogen bonding pattern for the five water molecules (W1–W5) inside the distal cavity.** Superimposed is the $F_o - F_c$ bromide difference map contoured at $\pm 4\ \sigma$, showing additional density at W2 corresponding to partial substitution by bromide. Small negative and larger positive features indicate a slight shift in the iron position.

included in the model at full occupancy and a round of X-PLOR refinement was carried out, residual maps showed no significant positive or negative density at this putative chloride site.

The chloride-binding site (Fig. 5) is composed of residues 324–327 at the amino terminus of the helix containing the proximal His^{336}, residues 30–33 of the small polypeptide, and Trp^{436}. These two stretches of polypeptide are in a parallel orientation and held together by two backbone hydrogen bonds. The chloride has three ligands: Trp^{32} NH, Val^{327} NH, and water in an almost planar trigonal arrangement. The water molecule is additionally hydrogen bonded to the peptide carbonyl oxygen of Leu^{33} and the guanidinium group NH of Arg^{31}. There are two tryptophans in the immediate vicinity of the chloride ion. Trp^{436} makes the closest approach with its indole ring CH_2 at a distance of 3.6 Å from the ion, whereas Trp^{32} is directed away from the ion with its C_γ 4.8 Å from the chloride.

Structure of an MPO-bromide Complex—To further characterize the binding properties of this site, an experiment was carried out to determine whether a second halide, bromide, could replace the putative chloride. As described above, x-ray diffraction data were recorded from a crystal soaked in 20 mM bromide at pH 5.5. A difference Fourier map, calculated using $F_{o\,(MPO\cdot bromide)} - F_{c\,(MPO)}$ coefficients revealed four separate bromide ions bound to each half of the molecule. The largest features of the map at 19.1 and 20.3 σ in the two halves of the molecule occur at the putative chloride-binding site (Fig. 5). Refinement indicated full occupancy by bromide at this site and residual maps showed no positive or negative features greater than 3 σ in this region. Superposition of the refined MPO-bromide model on that of the native revealed no significant protein conformational changes.

Two additional bromide ions were located at surface sites in each half of the molecule. Difference map peaks at 9.3 σ (A half) and 8.1 σ (B half) occur at water molecule 758, and peaks at 6.2 σ (A half) and 7.6 σ (B half) occur at water molecule 889. When these water molecules were replaced by bromide in the model, their occupancies refined to 0.60 and 0.54, respectively. Both of these ions are located well away from the heme group at distances of 29 and 26 Å from the heme iron. At the 889 position, the peptide NH groups of Gln^{201} and Phe^{213} together with a water molecule coordinate the bromide ion, whereas at 758, the peptide NH group of Thr^{544} and the guanidinium group of Arg^{382} are involved in bromide ligation.

Although there is no indication of bromide binding to the heme iron, difference map peaks of 5.2 σ (A half) and 5.9 σ (B half) occur in the distal heme cavity at the position of water

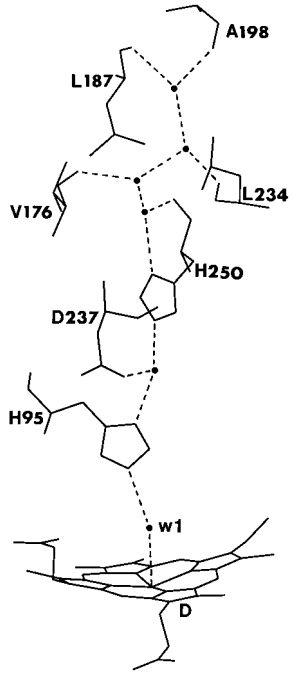

FIG. 4. **Diagram showing the five buried water molecules and His^{250} that form a chain of hydrogen bonds extending from the N_δ of the distal His^{95} to the surface of the molecule.**

molecule W2, which is hydrogen bonded to the amide nitrogen of Gln^{91} (Fig. 3). Bromide ions included in the model at this position refined to an occupancy of 0.44 in each half of the molecule. Superposition of the refined MPO-bromide and native models indicated small shifts of the side chains of the distal His^{95} and the heme ester linked Glu^{242} upon bromide binding. The side chain of Glu^{242}, which is only 3.5 Å away from W2 in the native enzyme, moves about 0.3 Å away from the bromide, and the His^{95} N_ϵ also moves about 0.2 Å away from the bound ion. Such movements are on the order of the expected level of error in the coordinates (0.2 Å, as determined from a Luzatti plot) and may not be significant. More significant movements of water molecules W1 and W5 by 0.35 and 0.45 Å away from the bromide were also seen.

The distal cavity bromide is located 0.3 Å from the position occupied by W2 in the native enzyme. Possible electrostatic interactions occur between the bromide and water molecules W1 and W5; the N_ϵ of His^{95} and the amide nitrogen of Gln^{91}

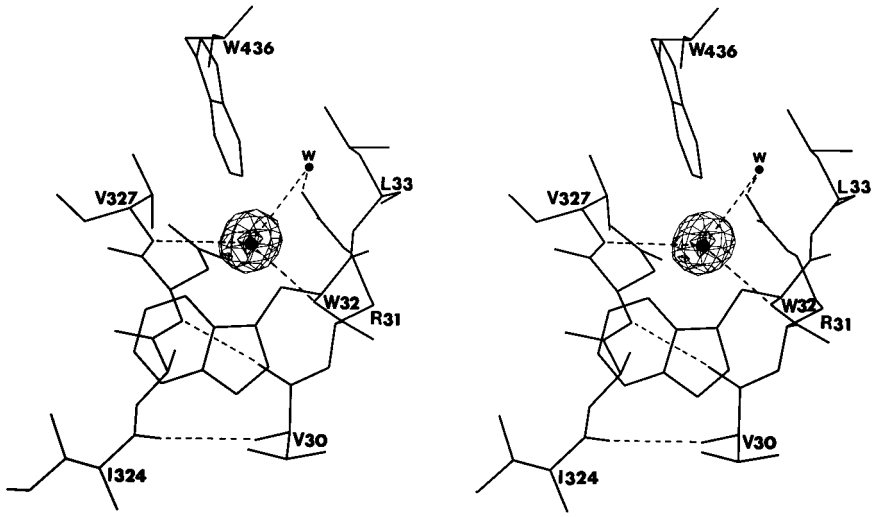

FIG. 5. **Stereo view of the proximal helix chloride-binding site in the native MPO model.** Residues 324–327 at the carboxyl terminus of the proximal helix are linked to residues 30–33 via two main chain hydrogen bonds. Superimposed is the $F_o - F_c$ bromide difference map contoured at 5 and 15 σ, showing additional density corresponding to replacement of chloride by bromide.

TABLE III
Halide interactions

From	To	Distance A	Distance B
		Å	
Native structure: proximal helix chloride			
Val^{327} NH	Cl^-	3.23	3.25
Trp^{32} NH	Cl^-	3.22	3.21
Wat^{652} OH	Cl^-	3.07	3.17
Bromide complex: proximal helix bromide			
Val^{327} NH	Br^-	3.36	3.50
Trp^{32} NH	Br^-	3.29	3.28
Wat^{652} OH	Br^-	3.32	3.30
Bromide complex: distal cavity bromide			
His^{95} N_ϵ	Br^-	3.55	3.50
Gln^{91} N_ϵ	Br^-	3.56	3.35
W1 OH	Br^-	3.12	3.20
W5 OH	Br^-	2.73	2.91
Heme Fe^{3+}	Br^-	5.04	4.99
Heme CHA	Br^-	3.80	3.77

(Table III). The closest heme atom to the bromide is the methylene bridge carbon between pyrrole rings A and D, at a distance of 3.8 Å, and the heme iron is at a distance of 5.0 Å. There does not appear to be any significant interaction between the bromide and the guanidinium group of the distal Arg^{239}. The C_δ of this residue makes the closest approach to the bromide at a distance of 3.95 Å and as indicated above, Arg^{239} is already involved in an ion pair interaction with Asp^{237}.

DISCUSSION

The mode of heme binding revealed by our studies may be unique to MPO. Although other members of this gene family all contain the conserved Asp^{94} and Glu^{242}, they lack methionine at position 243 (14). It is therefore likely that other mammalian peroxidases such as eosinophil peroxidase, LPO, and thyroid peroxidase also have heme-protein ester linkages analogous to those of MPO, but that the sulfonium ion linkage is a feature unique to MPO. It has been proposed by Kooter *et al.* (34, 35) that the sulfonium ion linkage should involve a bond between the Met sulfur atom and the α-carbon of the vinyl group, by analogy with the chemistry involved in the formation of thioether groups in cytochrome *c*. However, such a linkage is inconsistent with the high resolution crystal structure, which clearly shows (Fig. 2) that the link involves the vinyl β-carbon. Recently, it has been found that the formation of two ester bonds between the heme and polypeptide chain of LPO is a hydrogen peroxide-dependent autocatalytic process involving conversion of unmodified protoporphyrin IX to hydroxymethyl and di-hydroxymethyl intermediates presumably capable of ester bond formation with residues analogous to Asp^{94} and Glu^{242} of MPO (36). Difference Fourier transform infrared spectroscopic studies have confirmed the presence of two heme ester linkages in both LPO and MPO and have also indicated their presence in eosinophil peroxidase (37).

The Soret bands of the visible absorption spectra of mammalian peroxidases are characteristically red-shifted with respect to those seen in other heme proteins, and these spectral shifts have generally been ascribed to the influence of the protein environment on the spectral properties of the heme (12). In this regard it is noteworthy that a $Met^{243} \rightarrow$ Gln mutant of recombinant human MPO exhibits a Soret band at 410–412 nm, considerably blue-shifted from the 428-nm band of the native enzyme in its oxidized form (35, 37, 38). Similarly, a $Glu^{242} \rightarrow$ Gln mutant of MPO, presumably lacking one of the heme ester bonds, exhibits a blue-shifted Soret band at 416–418 nm, and an $Asp^{94} \rightarrow$ Asn mutant, presumed to lack the other ester bond, also has a blue-shifted Soret band at 414 nm (38, 39). These studies of mutants strongly suggest that the covalent linkages to the heme in MPO contribute to the observed red shifts of the Soret band in the visible absorption spectrum. There is evidence to suggest that the covalent linkages to the heme are important in maintaining the catalytic activities of mammalian peroxidases. The catalytic activity of recombinant LPO was shown to be dependent on the proportion of covalently bound heme in the enzyme, while mutants of MPO, in which residues involved in covalent heme attachment have been replaced, also exhibit catalytic properties markedly different from those of the native enzyme (36). Neither the $Met^{243} \rightarrow$ Gln nor the $Glu^{242} \rightarrow$ Gln mutant MPO was capable of catalyzing the peroxidation of chloride ion, and both mutants had reduced catalytic activities when substrates for the single electron oxidation reaction were used (35, 37, 39).

In both cytochrome *c* peroxidase and lignin peroxidase the N_δ of the distal histidine is hydrogen bonded to the amide carbonyl of Asn, and it has been proposed that this arrangement favors the imidazole tautomer in which the N_ϵ is free to accept a

proton from the peroxide substrate (40). In MPO the N_δ of His^{95} is hydrogen bonded to a buried water molecule, which is linked by His^{250} to a succession of four additional buried water molecules forming a chain of hydrogen bonds leading to the surface of the molecule. Such a chain could presumably also function to conduct protons away from the distal histidine and thereby ensure that the N_ϵ is free to accept a proton from peroxide.

Assignment of a bound chloride ion to account for the high electron density at the amino terminus of the proximal helix in the native enzyme is strongly supported by results showing that this site can also be occupied by bromide. However, we propose that the reported spectral changes that accompany halide binding to MPO result from halide binding to the site that we observe in the distal cavity. A number of factors support this hypothesis. First, the close proximity of this site to the heme is consistent with the potential for a bound anion to influence the electron distribution in the porphyrin ring, thereby inducing spectral changes. Second, the halide location, 3.5 to 3.6 Å from the distal His N_ϵ, is consistent with data indicating that halide binding is strongly influenced by the ionization state of a group on the enzyme with a pK of 4 to 4.5, which has been suggested to be the distal histidine (23, 24). At low pH, halide binding would be favored by charge-charge interaction between the protonated histidine and the halide anion. Third, the occupancy of halide binding in the distal cavity is consistent with the reported K_d values for both chloride and bromide binding to MPO (21). At pH 5.5, the K_d for chloride is on the order of 5 mM, whereas for bromide it is 20 mM. We have found that crystals of MPO soaked in 20 mM bromide at pH 5.5 contain bromide ion at 44% apparent occupancy at this site (note that the real occupancy must be less, because molecules that do not contain bromide presumably have water in this location). However, in the native enzyme structure, for which the mother liquor chloride concentration of 2 mM at pH 5.5 is less than half the reported K_d of 5 mM, chloride ion was not detected in the distal cavity. By the same reasoning, our data indicating that the proximal helix-binding site is fully occupied by both chloride in the native structure and by bromide in the complex, at the halide concentrations used, are inconsistent with its assignment as the site responsible for halide-induced spectral changes.

We propose that in resting MPO the distal cavity bromide-binding site corresponds to the site for inhibition of MPO by halides. Halide inhibition is competitive with respect to H_2O_2 (19–22), and the distal cavity bromide-binding site is only 3.5–3.6 Å from the N_ϵ of the distal histidine; sufficiently close to interfere with or even be mutually exclusive with H_2O_2 binding. Evidence from salicylhydroxamic acid binding to MPO (26) has suggested that the first step in compound I formation involves the formation of a hydrogen bond between H_2O_2 and the unprotonated N_ϵ of the distal histidine, prior to transfer of a proton to the histidine. The presence of a halide ion, in place of water molecule W2 in the distal cavity could interfere with the ability of the distal histidine to form a hydrogen bond with and/or accept a proton from H_2O_2.

Although several studies have concluded that there are separate sites on MPO for halide binding as substrate and as inhibitor (2, 3, 21, 22), others have concluded that there is only a single site (19, 23). Because of their remote locations from the heme, the two surface bromide-binding sites are unlikely to be involved in either inhibitor or substrate binding. Consideration can, however, be given to both the proximal helix site and the distal cavity site. A mechanism involving peroxidation at the proximal helix halide-binding site could involve a tryptophan free radical analogous to the Trp^{191} free radical associated with compound I of cytochrome *c* peroxidase, which is also located on the proximal side of the heme (41, 42). Although the MPO proximal helix halide-binding site includes two adjacent Trp residues, there have been no reports of signals indicative of amino acid free radicals in the EPR spectrum of MPO compound I. A fundamental difference between a catalytic mechanism involving halide substrate binding in the distal heme cavity as opposed to a remote site is the origin of the oxygen atom in the hypohalous acid product of the reaction. In the distal cavity, the ferryl oxygen of compound I, derived from H_2O_2 is the presumed source, whereas at a remote site a water molecule would be the most likely source. To our knowledge, the origin of this oxygen atom in the HOCl product of MPO catalyzed chloride peroxidation has not been established. At this time, a functional role for this site in the catalytic mechanism of MPO cannot be completely discounted, although a structural role such as stabilization of the proximal helix through charge-charge interaction with the positive helix dipole appears more likely.

Catalysis of halide peroxidation by MPO does not necessitate a halide substrate-binding site on the resting enzyme, because it is only necessary for halides to interact with compound I for peroxidation to occur. In this regard, it has previously been suggested that the cyanide complex of MPO may be a useful model for compound I, and one study has concluded that halide ions bind close to the heme in cyanide inhibited MPO (43). In compound I of MPO the distal cavity bromide-binding site should still be accessible to halides and could therefore also be the site at which halides bind as substrates. Model building, based on a ferryl oxygen to iron distance of 1.7 Å, indicates that a halide ion bound at this site would be about 3.6 Å from the heme ferryl oxygen and 3.8 Å from the heme methylene bridge carbon between pyrrole rings A and D, thereby readily facilitating electron transfer to the heme and incorporation of the ferryl oxygen into the hypohalous acid product of the reaction. In such a mechanism the distal histidine would play a dual role in catalysis; first in accepting a proton from hydrogen peroxide prior to scission of the O–O bond and second in suitably positioning the halide substrate for electron transfer to the heme of compound I and subsequent reaction with the ferryl oxygen.

Acknowledgment—We thank Lan Wang for assistance with the purification of human MPO.

REFERENCES

1. Agner, K. (1941) *Acta Chem. Scand.* **2,** (Suppl. 8) 1–62
2. Harrison, J. E., and Schultz, J. (1976) *J. Biol. Chem.* **251,** 1371–1374
3. Wever, R., Kast, W. M., Kasinoedin, J. H., and Boelens, R. (1982) *Biochim. Biophys. Acta* **709,** 212–219
4. Van Dalen, C. J., Whitehouse, M. W., Winterbourn, C. C., and Kettle, A. J. (1997) *Biochem. J.* **327,** 487–492
5. Klebanoff, S. J. (1970) *Science* **169,** 1095–1097
6. Belding, M. E., Klebanoff, S. J., and Ray, C. G. (1970) *Science* **167,** 195–196
7. Merlie, J. P., Fagan, D., Mudd, J., and Needleman, P. (1988) *J. Biol. Chem.* **263,** 3550–3553
8. Kimura, S., and Ikeda-Saito, M. (1988) *Proteins Struct. Funct. Genet.* **3,** 113–120
9. Cals, M. M., Maillart, P., Brignon, G., Anglade, P., and Dumas, B. R. (1991) *Eur. J. Biochem.* **198,** 733–739
10. Koeffler, H. P., Ranyard, J., and Pertcheck, M. (1985) *Blood* **65,** 484–491
11. Akin, D. T., and Kinkade, J. M., Jr. (1986) *J. Biol. Chem.* **261,** 8370–8375
12. Wever, R., and Plat, H. (1981) *Biochim. Biophys. Acta* **661,** 235–239
13. Andrews, P. C., and Krinsky, N. I. (1981) *J. Biol. Chem.* **256,** 4211–4218
14. Zeng, J., and Fenna, R. E. (1992) *J. Mol. Biol.* **226,** 185–207
15. Picot, D., Loll, P. J., and Garavito, M. (1994) *Nature* **367,** 243–249
16. Fenna, R., Zeng, J., and Davey, C. (1995) *Arch Biochem. Biophys.* **316,** 653–656
17. Taylor, K. L., Strobel, F., Yue, K. T., Ram, P., Pohl, J., Woods, A. S., and Kinkade, J. M., Jr. (1995) *Arch. Biochem. Biophys.* **316,** 635–642
18. Dolphin, D., Forman, A., Borg, D. C., and Felton, R. H. (1971) *Proc. Natl. Acad. Sci. U. S. A.* **68,** 614–618
19. Stelmaszynska, T., and Zgliczynski, J. M. (1974) *Eur. J. Biochem.* **45,** 305–312
20. Zgliczynski, J. M., Selvaraj, R. J., Paul, B. B., Stelmaszynska, T., Poskitt, P. K. F., and Sbarra, A. J. (1977) *Proc. Exp. Biol. And Med.* **154,** 418–422
21. Bakkenist, A. R. J., De Boer, J. E. G., Plat, H., and Wever, R. (1980) *Biochim. Biophys. Acta* **613,** 337–348
22. Andrews, P. C., and Krinsky, N. I. (1982) *J. Biol. Chem.* **257,** 13240–13245
23. Bolscher, B. G. J. M., and Wever, R. (1984) *Biochim. Biophys. Acta* **788,** 1–10

24. Ikeda-Saito, M. (1987) *Biochemistry* **26,** 4344–4349
25. Sutton, B. J., Little, C., Olsen, R. L., and Willassen, N. P. (1988) *J. Mol. Biol.* **199,** 395–396
26. Davey, C. A., and Fenna, R. E. (1996) *Biochemistry* **35,** 10967–10973
27. Otwinowski, Z. (1993) in *Proceedings of the CCP4 Study Weekend* (Sawyer, L., Isaacs, N., and Bailey, S., eds) pp. 56–62, Daresbury Laboratory, Warrington, England
28. Brunger, A. T. (1992) *X-PLOR*, version 3.1, Yale University Press, New Haven, CT
29. Engh, R. A., and Huber, R. (1991) *Acta Crystallogr.* **A 47,** 392–400
30. Brunger, A. T. (1992) *Nature* **355,** 472–474
31. Laskowski, R. A., MacArthur, M. W., Moss, D. S., and Thornton, J. M. (1992) *PROCHECK V2*, Oxford Molecular Ltd., Oxford, England
32. Johnson, K. R., Nauseef, W. M., Care, A., Weelock, M. J., Shane, S., Hudson, S., Koeffler, H. P., Selsted, M., Miller, C., and Rovera, G. (1987) *Nucleic Acids Res.* **15,** 2013–2028
33. Morishita, K., Kubota, N., Asano, S., Kaziro, Y., and Nagata, S. (1987) *J. Biol. Chem.* **262,** 3844–3851
34. Kooter, I. M., Pierik, A. J., Merkx, M., Averill, B. A., Moguilevsky, N., Bollen, A., and Wever, R. (1997) *J. Am. Chem. Soc.* **119,** 11542–11543
35. Kooter, I. M., Moguilevsky, N., Bollen, A., van der Veen, L. A., Otto, C., Dekker, H. L., and Wever, R. (1999) *J. Biol. Chem.* **274,** 26794–26802
36. De Pillis, G. D., Ozaki, S. I., Kuo, J. M., Maltby, D. A., and Ortiz de Montellano, P. R. (1997) *J. Biol. Chem.* **272,** 8857–8860
37. Kooter, I. M., Moguilevsky, N., Bollen, A., Sijtsems, N. M., Otto, C., and Wever, R. (1997) *J. Biol. Inorg. Chem.* **2,** 191–197
38. Jacquet, A., Garcia-Quintana, L., Deleersnyder, V., Fenna, R., Bollen, A., and Moguilevsky, N. (1994) *Biochem. Biophys. Res. Commun.* **202,** 73–81
39. Floris, R., Moguilevsky, N., Puppels, G., Jacquet, A., Renire, R., Bollen, A., and Wever, R. (1995) *J. Am. Chem. Soc.* **117,** 3907–3912
40. Poulos, T. L., and Fenna, R. E. (1994) *Metal Ions in Biological Systems* (Sigel, H., and Sigel, A., eds) Vol. 30, Chapter 2, pp. 26–75, Marcel Dekker, Inc., New York
41. Erman, J. E., Vitello, L. B., Mauro, J. M., and Kraut, J. (1989) *Biochemistry* **28,** 7992–7995
42. Yonetani, T., Schleyer, H., and Ehrenberg, A. (1976) *J. Biol. Chem.* **241,** 3240–3242
43. Lee, H. C., Booth, K. S., Caughey, W. S., and Ikeda-Saito, M. (1991) *Biochim. Biophys. Acta* **1076,** 317–320